Hydrodynamic transport properties of hard-sphere dispersions. I. Suspensions of freely mobile particles

R. J. Phillips[a] and J. F. Brady
Department of Chemical Engineering, California Institute of Technology, Pasadena, California 91125
G. Bossis
Laboratoire de Physique de la Matière Condensée, Université de Nice, Parc Valrose, 06034 Nice Cedex, France

(Received 8 March 1988; accepted 24 August 1988)

The hydrodynamic transport properties of hard-sphere dispersions are calculated for volume fractions (ϕ) spanning the dilute limit up to the fluid–solid transition at $\phi = 0.49$. Particle distributions are generated by a Monte Carlo technique and the hydrodynamic interactions are calculated by Stokesian dynamics simulation. The effects of changing the number of particles in the simulation cell are investigated, and the scaling laws for the finite-size effects are derived. The effects of using various levels of approximation in computing both the far- and near-field hydrodynamic interactions are also examined. The transport properties associated with freely mobile suspensions—sedimentation velocities, self-diffusion coefficients, and effective viscosities—are determined here, while the corresponding properties of porous media are determined in a companion paper [Phys. Fluids **31**, 3473 (1988)]. Comparison of the simulation results is made with both experiment and theory. In particular, the short-time self-diffusion coefficients and the suspension viscosities are in excellent agreement with experiment.

I. INTRODUCTION

Recent developments in the fluid mechanics of particulate systems have made it possible to advance significantly our understanding of how the bulk properties of a suspension are determined by its microstructure. The solution to the theoretical problem of two spheres interacting under conditions of low particle Reynolds number[1,2] has made an important contribution to these efforts, principally through the application of pairwise additivity assumptions. Examples of the application of pairwise additivity in the study of suspension mechanics are Batchelor's[3,4] and the Glendinning–Russel[5] calculations of sedimentation velocities and self-diffusion coefficients for suspensions, the Batchelor–Green[6] calculation of the $O(\phi^2)$ coefficient for the effective viscosity of a suspension with volume fraction $\phi \ll 1$, and the development of Brady and Bossis,[7] of a method for simulating the trajectories of spherical particles suspended in a shear flow. It should be noted, however, that the pairwise additivity used by Brady and Bossis was an additivity of forces, rather than the additivity of velocities used by other workers (in the framework of Sec. III, an additivity of resistance, as opposed to mobility, interactions).

Recently, Durlofsky *et al.*[8] have improved upon the purely pairwise additive approach of Brady and Bossis by proposing a method that includes many-body, far-field interactions among finite numbers of spheres and uses pairwise additivity only to account for near-field, or lubrication interactions. Short-range lubrication interactions are only two-body effects, and thus the method of Durlofsky *et al.* is remarkably accurate. Brady *et al.*[9] have since extended this method for use in simulating infinite suspensions of particles, and this modified theory, which goes under the name of Stokesian dynamics, was shown to produce results that compare favorably with known exact solutions[10–12] for the permeabilities, spin viscosities, and shear viscosities of cubic lattices of spheres. A summary of the general Stokesian dynamics method is given in Brady and Bossis.[13]

One advantage of the Stokesian dynamics method proposed by Brady *et al.* is that it places no restrictions on the locations of the particles other than those required by the imposition of periodic boundary conditions. Thus it can be readily applied either to dynamic simulations, in which particle trajectories are followed over time, or to Monte Carlo simulations, in which transport properties for instantaneous configurations of particles are calculated and averaged over several realizations. Furthermore, the Stokesian dynamics method allows the simultaneous investigation of sedimentation, permeability, rheology, diffusion, etc.; any and all hydrodynamic properties can be determined for any microstructural arrangement of spherical particles.

In this paper we present the results of a series of Monte Carlo simulations from which the transport properties of unbounded, disordered systems of hard spheres were determined. (Dynamic simulation studies are discussed in Refs. 7 and 13–17.) The hard-sphere distribution represents a convenient reference microstructure in that it is often amenable to analytical analysis, even though it might not be the microstructure obtained by any particular suspension of spherical Brownian particles. Results for those properties that one normally associates with particulate suspensions, such as sedimentation velocities, short-time coefficients of self-diffusion, and effective viscosities, will be given in this paper. In a companion paper,[18] we shall present the corresponding properties of porous media, such as permeabilities and short-time coefficients of hindered diffusion.

Calculations have been carried out over volume fractions ranging from infinite dilution up to the fluid–solid

[a]Present address: Department of Chemical Engineering, Massachusetts Institute of Technology, Cambridge, Massachusetts 02139.

 0031-9171/88/123462-11$01.90

transition, which occurs at approximately $\phi = 0.49$ for hard spheres.[19] In addition, we compare the effects of three different levels of approximation in modeling the hydrodynamic interactions, and we examine the effect of changing the length scale over which we impose periodic boundary conditions in modeling the infinite nature of the dispersions, thereby obtaining the scaling laws for finite-size effects. In all cases where it is possible, we compare our results both with alternative theories and with experimental data, thereby providing some criteria for assessing the accuracy of our method. For the cases of the short-time self-diffusion coefficient and the high-frequency dynamic viscosity of a Brownian suspension, for which the hard-sphere microstructure is the proper microstructure, our simulation results are in excellent agreement with experiment.[20–22]

The Monte Carlo approach used to perform these simulations consisted of generating several samples, calculating the transport properties of interest for each sample, and then averaging in order to obtain values describing the macroscopic behavior of the suspension. In the next section we describe our sample-generating techniques. This is followed by Sec. III, which gives a brief description of the Stokesian dynamics method and the averages used to define the macroscopic properties. In Sec. IV our results are presented, analyzed, and compared with theory and experiment. Finally, we conclude with an examination of the implications of this work for future research involving simulations of hydrodynamically interacting particles.

II. SAMPLING TECHNIQUES

The procedure used to generate the hard-sphere microstructure varied according to the volume fraction of the suspension. For $\phi < 0.25$, sphere locations within the periodic, simple cubic unit cell were chosen by random sequential addition. For $0.25 < \phi < 0.49$, the spheres were placed in an arbitrary initial configuration and then moved using a random-stepping routine in order to ensure that the sample was disordered. To check that the samples generated using the latter, random-stepping method were sufficiently randomized, and that one configuration was statistically independent from another, the linear correlation between the initial and final coordinates ($\mathbf{x}$) of the particles was monitored through the correlation coefficient r_c. For example, the correlation between particle positions in two samples **A** and **B** could be checked by plotting $\mathbf{x}_A$ vs $\mathbf{x}_B$ for the N particles, and then calculating the three linear correlation coefficients. If the particles had not moved significantly from their previous positions, then one would expect values of r_c close to unity, whereas sufficient randomization should result in a much lower level of correlation. Because this method of monitoring spatial correlation is only approximate and is based primarily on intuitive arguments, we accepted $r_c < 0.5$ as being a reasonable criterion for statistical independence and did not attempt a rigorous statistical analysis.

For $\phi = 0.25$ this criterion was easily met by moving each particle 500 steps between samples, where the length of each step was chosen so that the probability of success (i.e., no overlap) was about 0.5–0.7, values that agree closely with those suggested by Binder.[23] Radial distribution functions calculated from samples used in our calculations of hydrodynamic transport properties generally agreed with those of Barker and Henderson,[24] to within 10%, although the maximum values at contact were sometimes in error by as much as 20%. Using more than ten samples produced excellent radial distribution functions. To check the consistency of the two sample-generating methods used, we performed simulations using each of them at $\phi = 0.25$ and found that the two sets of results did not differ significantly. In addition, our results at $\phi = 0.40$ were found to be independent of the initial configuration chosen and did not change when the number of randomization steps was doubled from 500 to 1000 steps per particle.

III. HYDRODYNAMIC TRANSPORT PROPERTIES BY STOKESIAN DYNAMICS

Once the locations of the N particles are specified, the transport properties can be determined by Stokesian dynamics. We begin by forming the grand mobility matrix $\mathcal{M}$, which relates the kinematic and dynamic quantities of interest[9]:

$$\begin{pmatrix} \mathbf{U} - \langle \mathbf{u} \rangle \\ -\langle \mathbf{E} \rangle \end{pmatrix} = \begin{pmatrix} \mathbf{M}_{UF} & \mathbf{M}_{US} \\ \mathbf{M}_{EF} & \mathbf{M}_{US} \end{pmatrix} \cdot \begin{pmatrix} \mathbf{F} \\ \mathbf{S} \end{pmatrix}. \tag{1}$$

Here, $\mathbf{U} - \langle \mathbf{u} \rangle$ is a vector of dimension $6N$ containing the translational and rotational velocities of all N particles relative to the *suspension average* velocity $\langle \mathbf{u} \rangle$, $\langle \mathbf{E} \rangle$ is a vector of dimension $5N$ that repeats the suspension average rate of strain for each particle, $\mathbf{F}$ is a $6N$ vector containing the force and torque exerted by the particles on the fluid, and $\mathbf{S}$ is of dimension $5N$ and contains the particle stresslets (the symmetric and traceless portion of the first moment of the force distribution integrated over the particle surfaces). The submatrices of the grand mobility matrix give the coupling of the kinematic ($\mathbf{U}$) and dynamic ($\mathbf{F}$) quantities: $\mathbf{M}_{UF}$ relates particle velocities to forces and torques, $\mathbf{M}_{US}$ relates velocities to stresslets, $\mathbf{M}_{EF}$ relates the rate of strain to the forces and torques, and $\mathbf{M}_{ES}$ relates the rate of strain and the stresslets. The only assumption made in writing (1) is that the particle Reynolds number is small.

Inverting the grand mobility matrix $\mathcal{M}$ in (1) results in the grand resistance matrix $\mathcal{R}$ that relates $\mathbf{F}$ and $\mathbf{S}$ to $\mathbf{U}$ and $\mathbf{E}$:

$$\begin{pmatrix} \mathbf{F} \\ \mathbf{S} \end{pmatrix} = \begin{pmatrix} \mathbf{R}_{FU} & \mathbf{R}_{FE} \\ \mathbf{R}_{SU} & \mathbf{R}_{SE} \end{pmatrix} \cdot \begin{pmatrix} \mathbf{U} - \langle \mathbf{u} \rangle \\ -\langle \mathbf{E} \rangle \end{pmatrix}. \tag{2}$$

The grand resistance matrix has been partitioned in the same manner as was the grand mobility matrix $\mathcal{M}$. Both $\mathcal{M}$ and $\mathcal{R}$ are symmetric and positive definite, owing to the dissipative nature of Stokes flow.

We have written the translational and rotational velocities and the forces and torques together as a single vector for convenience. It should be appreciated, however, that the matrix $\mathbf{R}_{FU}$ (as well as $\mathbf{M}_{UF}$) can be further partitioned into submatrices if we write out explicitly the force and torque:

$$\begin{pmatrix} \hat{\mathbf{F}} \\ \mathbf{L} \end{pmatrix} = \begin{pmatrix} \hat{\mathbf{R}}_{FU} & \mathbf{R}_{F\Omega} \\ \mathbf{R}_{LU} & \mathbf{R}_{L\Omega} \end{pmatrix} \cdot \begin{pmatrix} \mathbf{U} - \langle \mathbf{u} \rangle \\ \boldsymbol{\Omega} - \langle \boldsymbol{\omega} \rangle \end{pmatrix}. \tag{3}$$

Here, $\mathbf{L}$ is the torque exerted by the particles on the fluid, and

$\boldsymbol{\Omega} - \langle\boldsymbol{\omega}\rangle$ is the particles' angular velocity ($\boldsymbol{\Omega}$) relative to the suspension average velocity ($\langle\boldsymbol{\omega}\rangle$). In a similar fashion, $\mathbf{R}_{FE}$ can be further partitioned into ($\hat{\mathbf{R}}_{FE}$ $\mathbf{R}_{LE}$). We shall use the shortened notation of (1) and (2) unless otherwise stated. Where necessary, we shall break $\mathbf{R}_{FU}$ in (2) into its submatrices in (3), and hope that no confusion will arise with the use of the subscript FU in the different contexts of (2) and (3). We have placed a caret above the force and the matrix that couples the force only, as opposed to the larger matrix without the caret that couples both force and torque.

The construction of the mobility and resistance matrices is discussed in detail in Brady *et al.*,[9] and so will not be repeated for the sake of brevity. We will, however, summarize the essential features of our approach in order to explain the significance of the levels of hydrodynamic interactions used in the calculations presented in Sec. IV. The grand mobility matrix $\mathcal{M}$ in (1) is approximated by a far-field, multipole expansion in powers of $1/r$, where r is the distance between two particles. Care is taken to sum all the long-range hydrodynamic interactions properly for the N periodically replicated particles by using O'Brien's method[25] of renormalization together with the Ewald summation technique. The Ewald-summed, far-field mobility matrix is denoted by $\mathcal{M}^*$.

As discussed by Brady *et al.*,[9] the near-field lubrication interactions, which become progressively more important as particles move closer together, are included via the resistance matrix in a pairwise additive fashion, thereby making use of the short-range nature of these interactions. Thus the approximation to the true resistance matrix, including both far-field, many-body interactions and near-field, lubrication effects, is

$$\mathcal{R}^* = (\mathcal{M}^*)^{-1} + \mathcal{R}_{\text{lub}}. \tag{4}$$

Once formed, the grand resistance matrix can be partitioned as in (2) for use in calculating transport properties.

We shall compare various levels of hydrodynamic approximations in our discussion of hydrodynamic transport properties. First, there are three different levels at which we can form the mobility matrix before inversion. If only the translational velocity-force couplings are used in the far-field mobility matrix, then

$$(\hat{\mathcal{M}}^*)_{FU}^{-1} = (\hat{\mathbf{M}}^*_{UF})^{-1}, \tag{5a}$$

where one needs the $\mathbf{M}_{UF}$ matrix of (1) to be further partitioned into submatrices as in (3). If the complete translational/rotational velocity force/torque couplings are used, then the far-field mobility matrix is given by

$$(\mathcal{M}^*)_{FU}^{-1} = (\mathbf{M}^*_{UF})^{-1}. \tag{5b}$$

Using (5a) results in what we shall refer to as the "F (force) method," while using (5b) describes what we call the "F–T (force–torque) method." Inverting the full, far-field grand mobility matrix $\mathcal{M}^*$ of (1) results in the most accurate of the three methods, the so-called "F–T–S (force–torque–stresslet) method."[26]

The lubrication matrix, $\mathcal{R}_{\text{lub}}$, is formed by inverting a two-body, F–T–S mobility matrix containing only far-field interaction terms and subtracting the invert from the complete two-body resistance matrix, thereby leaving only near-field interactions. More detailed information concerning the formation of $\mathcal{M}^*$ and $\mathcal{R}_{\text{lub}}$ can be found in Refs. 8 and 9. Note that the size of the mobility matrix that must be inverted in (4) increases from $3N \times 3N$ to $6N \times 6N$ and then to $11N \times 11N$ as one progresses from the F to the F–T to the F–T–S method. Since the time required to invert a matrix grows as the cube of the matrix dimension, it is clearly desirable to have some idea of how the three methods compare in terms of accuracy, and therein lies one motivation for the comparisons that will be made in the next section. Also, in addition to comparing the levels of hydrodynamic interactions used in forming the far-field mobility matrices, we shall compare results with and without lubrication effects, thereby assessing the importance of the near-field interactions.

All the information needed to calculate the macroscopic transport properties of the dispersion are contained in the mobility and/or resistance matrices. The definitions and averages for the hydrodynamic transport properties for suspensions of freely mobile particles will be presented here; for a discussion of porous media, see Ref. 18.

The sedimentation velocity of a suspension $\langle\mathbf{U}\rangle$, is usually defined as the average translational velocity of the particles relative to zero volume flux axes, i.e., such that the *suspension average* velocity ($\langle\mathbf{u}\rangle$) is zero. The angle brackets defining the average denote a sum over all particles (assumed identical here) and an average over all realizations of the suspension microstructure:

$$\langle\mathbf{U}\rangle = \frac{1}{T}\sum_{t=1}^{T}\frac{1}{N}\sum_{\alpha=1}^{N}\mathbf{U}^{\alpha},$$

where α labels one of the N particles and t labels a realization of the microstructure. From the grand resistance matrix in (2) we have, with no imposed shear flow ($\langle\mathbf{E}\rangle = 0$),

$$\langle\mathbf{U}\rangle = \langle\mathbf{R}^{*}_{FU}{}^{-1}\cdot\mathbf{F}\rangle = \langle\mathbf{R}^{*-1}_{FU}\rangle\cdot\mathbf{F}, \tag{6}$$

where the last equality comes from the fact that all particles are identical.

Since our definitions of $\mathbf{U}$ and $\mathbf{F}$ contain both translational and rotational parts, Eq. (6) defines both the sedimentation velocity, or the translational velocity resulting from a force with no applied torque, and the "rotational velocity," or the angular velocity resulting from a torque with no applied force. Written out in terms of the submatrices of (3), (6) becomes

$$\begin{pmatrix}\langle\mathbf{U}\rangle\\ \langle\boldsymbol{\Omega}\rangle\end{pmatrix} = \left\langle\begin{pmatrix}\hat{\mathbf{R}}^{*}_{FU} & \mathbf{R}^{*}_{F\Omega}\\ \mathbf{R}^{*}_{LU} & \mathbf{R}^{*}_{L\Omega}\end{pmatrix}^{-1}\right\rangle\cdot\begin{pmatrix}\hat{\mathbf{F}}\\ \mathbf{L}\end{pmatrix}. \tag{7}$$

The average sedimentation velocity, which we denote by $\mathbf{U}_s$, is obtained by setting $\mathbf{L} = \mathbf{0}$, while the average rotational velocity, which we denote by $\boldsymbol{\Omega}_s$, is obtained by setting $\hat{\mathbf{F}} = \mathbf{0}$. Note that these properties are averages of the entire mobility matrix [shown in (7) as the inverse of the resistance matrix].

In an isotropic, statistically homogeneous media such as that obtained here for the hard-sphere distribution $\langle\mathbf{R}^{*}_{FU}{}^{-1}\rangle$ is proportional to the isotropic unit tensor $\mathbf{I}$, giving scalar coefficients of sedimentation and rotation:

$$\mathbf{U}_s = U_s\hat{\mathbf{F}}, \tag{8a}$$

$$\boldsymbol{\Omega}_s = \Omega_s\mathbf{L}. \tag{8b}$$

The cross terms in (7) vanish upon averaging. Although

there are only scalar coefficients of average sedimentation and rotation, each realization of the suspension microstructure produces three separate values for each coefficient, corresponding to a force (torque) in each of the three orthogonal directions. Thus the statistical averaging over realizations is augmented by a factor of 3. As a final note, in the dilute limit where $\phi \to 0$, we have Stokes' law giving $\mathbf{U}_s = \mathbf{F}/(6\pi\eta a)$ and $\mathbf{\Omega}_s = \mathbf{L}/(8\pi\eta a^3)$.

The procedure for calculating the short-time self-diffusion coefficients for a sphere in a suspension of force-free, torque-free particles is very similar to that outlined above. In this case, however, instead of all the spheres having the same applied force, only the sphere whose mobility is being calculated has a nonzero force. The coefficients relating the velocity and force lie along the diagonal of $\mathbf{R}_{FU}^{*\,-1}$. Averaging these diagonal elements therefore corresponds to applying a force separately to each sphere in turn, calculating its velocity to obtain its self-mobility, and then averaging these self-mobilities. Note that this average is being performed over instantaneous configurations of the particles—that is, the time scale for the measurement is so short that the particles do not move a distance comparable to their own size or to the interparticle spacing. Thus the average corresponds to the short-time diffusivity. The long-time self-diffusivity, where a particle moves far from its starting point, can only be obtained through dynamic simulation.[17]

The short-time self-diffusivities are defined through the Stokes–Einstein relation by

$$\mathbf{D}_0^s = kT\langle \mathrm{tr}(\mathbf{R}_{FU}^{*\,-1})\rangle, \tag{9}$$

where we define a trace operator tr that picks out only the diagonal elements of $\mathbf{R}_{FU}^{*\,-1}$ (which are 3×3 matrices). As before, the angle brackets imply a sum over all particles and an average over all configurations. Also, k is Boltzmann's constant, and T is the absolute temperature. Just as Eq. (6) contains both translational and rotational parts, so does (9) contain translational and rotational diffusivities. We denote the scalar translational and rotational diffusivities by D_0^s and D_r^s, respectively. Again, each realization of the suspension gives three separate values for D_0^s and D_r^s. In the dilute limit where $\phi \to 0$ we have $D_0^s = kT/(6\pi\eta a)$ and $D_r^s = kT/(8\pi\eta a^3)$.

The final property we will discuss concerning freely mobile suspensions is the shear viscosity. The shear, or effective, viscosity is defined through a calculation of the bulk deviatoric stress from the following expression[6,9,13]:

$$\langle \mathbf{\Sigma}\rangle - \tfrac{1}{3}\mathbf{I}:\langle \mathbf{\Sigma}\rangle \mathbf{I} = 2\eta\langle \mathbf{E}\rangle - n\langle \mathbf{S}\rangle, \tag{10}$$

where $\langle \mathbf{\Sigma}\rangle$ is the average, macroscopic stress, η is the viscosity of the fluid, and n is the number density of particles. Here $\langle \mathbf{S}\rangle$ is the particle average stresslet for force- and torque-free particles and is linearly related to the average rate of strain $\langle \mathbf{E}\rangle$ by a fourth-order tensor $\mathbf{A}$,

$$\langle \mathbf{S}\rangle = +\mathbf{A}:\langle \mathbf{E}\rangle, \tag{11a}$$

where, from (2), $\mathbf{A}$ is given by

$$\mathbf{A} = \langle \mathbf{R}_{SU}^{*}\cdot\mathbf{R}_{FU}^{*\,-1}\cdot\mathbf{R}_{FE}^{*} - \mathbf{R}_{SE}^{*}\rangle. \tag{11b}$$

For the isotropic, hard-sphere distribution, the symmetric and traceless $\mathbf{A}$ must be of the form

$$A_{ijkl} = (\beta/2)(\delta_{ik}\,\delta_{jl} + \delta_{il}\,\delta_{jk} - \tfrac{2}{3}\,\delta_{ij}\,\delta_{kl}), \tag{12}$$

where β is a function of the volume fraction ϕ alone. With the normalization $\frac{20}{3}\pi\eta a^3$ for the stresslets, the relative viscosity η_r, defined as the suspension viscosity divided by the fluid viscosity, is given by

$$\eta_r = 1 + \tfrac{5}{2}\phi\beta. \tag{13}$$

In the dilute limit $\phi \to 0, \beta \sim 1 + O(\phi)$, and we recover Einstein's viscosity. There are five independent components of $\mathbf{A}$, and thus for each realization we obtain five values of η_r, thereby improving the accuracy of our results.

All of the calculations described here were done on a CYBER 205 supercomputer. It required 22 seconds of CPU time to fill the complete, Ewald-summed, F–T–S mobility matrix for a single 27 sphere sample, while six seconds were required to invert that matrix. The CPU time required to form $\mathscr{R}_{\mathrm{lub}}$ is negligible compared to that needed for the formation and inversion of $\mathscr{M}^*$. Although these requirements might seem prohibitive to those interested in doing dynamic simulations, we should point out that suitable, time-saving approximations can be used to significantly decrease the time requirements of this method. Two such possibilities are (a) only recalculating far-field interactions on a time scale that allows for the particles to move a significant fraction of their own radii, such as every 10 or 100 time steps, or (b) using the less accurate F or F–T methods to take advantage of the corresponding reduction in the size of the mobility matrix. The former approximation is made possible by the fact that far-field interactions are insensitive to small rearrangements in the system configuration, while some information on the implications of the latter approximation will be obtained by examining the results of Sec. IV. Either or both of these suggestions could be of potential value, depending upon the particular problem being investigated.

For this work, computer time limitations required us to perform averages over only ten samples for each volume fraction. Fortunately, however, 95% confidence intervals calculated using the standard deviations associated with the data were generally within 5% of the average values reported. As discussed previously, the statistical errors were decreased by the fact that each sample produces five values for the viscosity and three values for the sedimentation velocity, self-diffusion coefficient, rotational velocity, and rotational diffusion coefficient. Thus although only ten samples are represented in each data point, that point is actually an average computed from either 30 or 50 values, depending on the transport property in question.

IV. RESULTS AND DISCUSSION

The significance of our results for disordered systems can be viewed from several perspectives. As was stated earlier, the effects of the approximations made in our hydrodynamic theory have already been tested by Brady *et al.* in their comparison of the results of the method used here with known results for cubic arrays of spheres. Examining disordered systems will allow us to further test this method by comparing both with a different set of theoretical results and with experimental data. It should be noted, however, that an

exhaustive comparison with theory is not attempted, as the large number of such theories makes such an undertaking unfeasible. In addition to these comparisons, the effects of imposing periodic boundary conditions, which pose no ambiguities when modeling a periodic system, can be significant in calculations involving disordered media. Thus the results presented in the following paragraphs should both demonstrate the application of the newly derived theory and give the reader some indication of the effects of long-range order on disordered systems.

The results are organized in the following manner. The sedimentation velocity and the short-time diffusion coefficient data are presented in Secs. IV A and IV B, where we also provide a discussion of the effects of using a finite number of particles (N) to represent an infinite system. In Sec. IV C we discuss the rotational velocity and short-time rotational diffusion coefficient. Finally, in Sec. IV D we discuss the effective viscosity results.

A. Sedimentation velocity

The complications associated with inserting some degree of periodicity into a model of a disordered medium are relatively severe in the sedimentation problem. To understand why this is the case, one must look more closely at exactly what problem is being solved in our simulation. Although we are attempting to model a random, sedimenting suspension, what we actually have, as a result of the imposed periodic boundary conditions, are N simple cubic lattices of spheres sedimenting among one another. Each sphere "sees" the $N-1$ other sphere positions evenly distributed throughout its periodic box as a result of the averaging that takes place in the Monte Carlo simulations. Thus our sedimenting suspension has both periodic and random characteristics.

To assess the relative importance of these two components, we can examine the dependence of the asymptotic, low volume fraction solutions for U_s associated with both periodic and random systems. For a random suspension, we have from Batchelor,[3] to leading order in ϕ,

$$U_s^{\text{ran}} = 1 - 6.55\phi, \tag{14}$$

while for a suspension of particles in a simple cubic (SC) lattice, Saffman[27] gives

$$U_s^{\text{SC}} = 1 - 1.74\phi^{1/3}. \tag{15}$$

The $\phi^{1/3}$ dependence of the sedimentation coefficient for periodic lattices suggests that periodic characteristics of our system are likely to be important, particularly at low volume fractions. The sedimentation velocities in (14) and (15) have been normalized by U_s^0, the sedimentation velocity of an isolated sphere in an unbounded fluid.

A simple approach to determining how the effects of periodicity scale with N is to assume that we have a simple cubic lattice of volume fraction ϕ/N sedimenting superimposed on a random, sedimenting suspension of volume fraction $\phi(1-1/N)$. That these two effects are superimposable can be shown by considering the calculations of the Ewald sums used in constructing $\hat{\mathbf{M}}_{UF}^{*}$ in the grand mobility matrix of Eq. (1). Thus the sedimentation velocity at dilute ϕ should be approximately given by

$$U_s \approx 1 - 1.74\phi^{1/3}N^{-1/3} - 6.55\phi(1-N^{-1}). \tag{16}$$

The finite-size effects and the effects of periodicity should thus decay as $N^{-1/3}$, which is quite slow. From a different perspective, if the periodicity effects are to be small compared to the random results, then we have the requirement

$$N \gg \phi^{-2}, \tag{17}$$

a condition which is extremely severe as $\phi \to 0$.

In Fig. 1 the results of our simulations with N values of

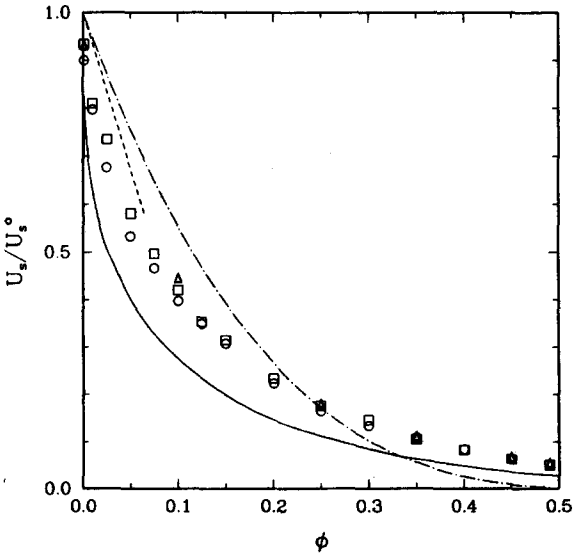

FIG. 1. The sedimentation velocity, nondimensionalized by the infinite dilution value U_s^0, is plotted versus the volume fraction (ϕ) for several different cases. The open symbols correspond to the Stokesian dynamics results for 14 (○), 27 (□), and 64 (△) spheres in the unit cell. The solid curve is the exact result for simple cubic lattices (Ref. 10), the dashed–dotted curve is a correlation of experimental data (Ref. 28), and the dotted curve is the low ϕ asymptotic result of Batchelor (Ref. 3).

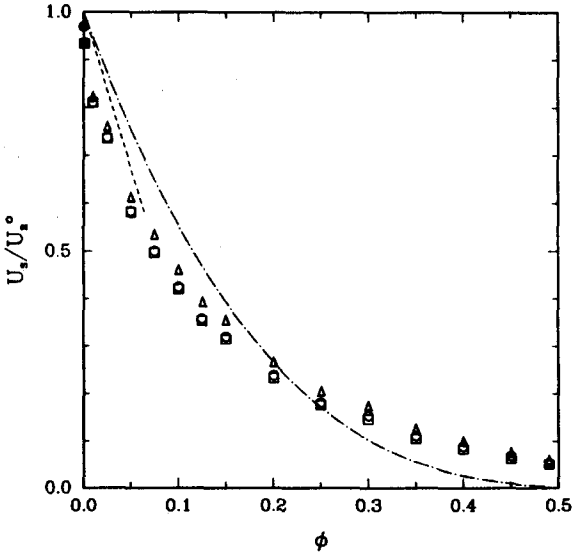

FIG. 2. Comparison of various levels of hydrodynamic approximation on the sedimentation velocity. The open squares are for 27 particles using the full F–T–S method with lubrication. The open triangles are results for the F method (i.e., no stresslets, but including lubrication), and the open circles are the F–T–S method results without lubrication. The curves are the same as in Fig. 1. These results show that induced stresslet interactions and lubrication play no significant role in sedimentation.

14, 27, and 64 spheres are plotted along with the results of Zick and Homsy[10] for an SC lattice and Batchelor's low volume fraction result. The influence of periodicity is clearly evident and, as one might expect, tends to be more severe for the 14 sphere simulations than for the 27 and 64 sphere simulations. Unfortunately, however, there was no discernible trend with the 27 and 64 sphere samples and thus an extrapolation to infinite N was not possible. Also included in Fig. 1 is a correlation of experimental data reported by Buscall *et al.*,[28] who measured sedimentation velocities for suspensions of polystyrene lattices. Note that the $O(\phi)$ coefficient obtained by taking the slope of the experimental data, roughly 5.4, differs from that predicted by Batchelor [cf. Eq. (14)]. The roots of this discrepancy are explained in Brady and Durlofsky.[29]

In Fig. 2 the results for our 27 sphere simulations using the F method, the F–T–S method, and the F–T–S method without lubrication [i.e., without $\mathcal{R}_{\text{lub}}$ in (4)] are presented. The F–T method results were essentially identical to those for the F method, and so were left out for simplicity. Perhaps the most interesting conclusion to be drawn from this plot is that the near-field interactions have virtually no effect on the sedimentation velocity. The explanation for this effect has been given in detail in Brady *et al.*[9] and in Brady and Durlofsky. Quite simply, the fluid displaced by the falling particles flows up through the interstices between particles. Little fluid flows between the narrow gaps separating the particle surfaces at high ϕ, and therefore the lubrication forces do not come into play. The only way to obtain better agreement with experiment at high ϕ is to include higher multipole moments in the development of the grand mobility matrix in Eq. (1). Indeed, since the odd moments are zero on average because of symmetry, one must include as far as the hexadecapole to obtain 10% accuracy at $\phi = 0.5$ (cf. Brady *et al.*[9]).

Thus the small number of particles used here makes the effects of periodicity dominate the sedimentation velocity at small ϕ, and the relatively low number of multipoles included reduces the accuracy at high ϕ. Improvements can be made on both fronts by including more multipoles on the one hand and more particles on the other. Either of these approaches, however, increases dramatically the number of unknowns or degrees of freedom and results in prohibitive computation times. Even if the F method is used without lubrication, thereby avoiding the costly $O(N^3)$ inversion, calculating the mobility interactions requires $O(N^2)$ operations, which is still excessive at small ϕ in light of the criterion given in (17).

B. Short-time self-diffusion coefficient

The periodicity problems that plagued the sedimentation velocity results are also present in the calculation of the short-time self-diffusion coefficient. In this case, however, the data follow a perceptible trend with increasing N, so that an extrapolation to obtain the limiting behavior as $N \to \infty$ is possible. To derive the dependence of D_0^s on N, we recall that in calculating the self-diffusion coefficient, or self-mobility, one is essentially exerting a force on one sphere and calculating its resulting velocity. Because of the periodic boundary conditions, however, a force exerted on one sphere is also exerted on all the images of that sphere. We thus have, again, a simple cubic lattice of volume fraction ϕ/N "sedimenting" in superposition with the motion of one particle in $N-1$ neutrally buoyant particles. Hence the analysis leading to (16) is applicable, with Batchelor's[4] calculation of the self-diffusion coefficient for a random suspension,

$$D_0^s = 1 - 1.83\phi, \tag{18}$$

replacing (14). We expect therefore an $N^{-1/3}$ scaling in our data. Here, D_0^s has been nondimensionalized by the diffu-

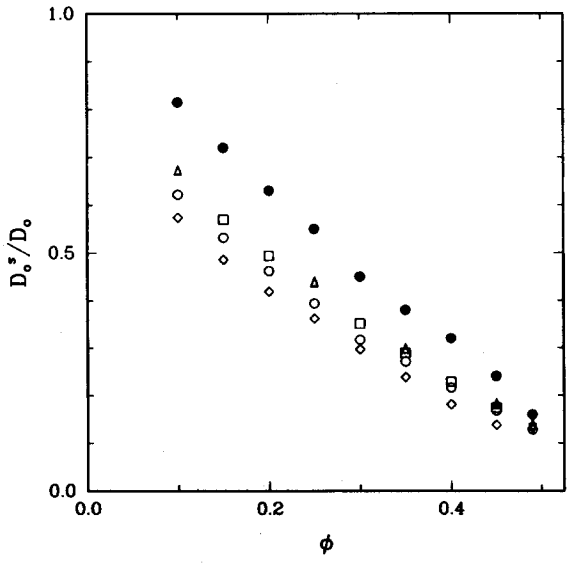

FIG. 3. The short-time self-diffusion coefficient normalized by its infinite dilution value, $D_0 = kT/(6\pi\eta a)$, is plotted as a function of volume fraction (ϕ) for different numbers of particles in the unit cell (open symbols). The solid symbols are the values obtained by extrapolation to infinite N based on the $N^{-1/3}$ scaling derived in Eq. (16).

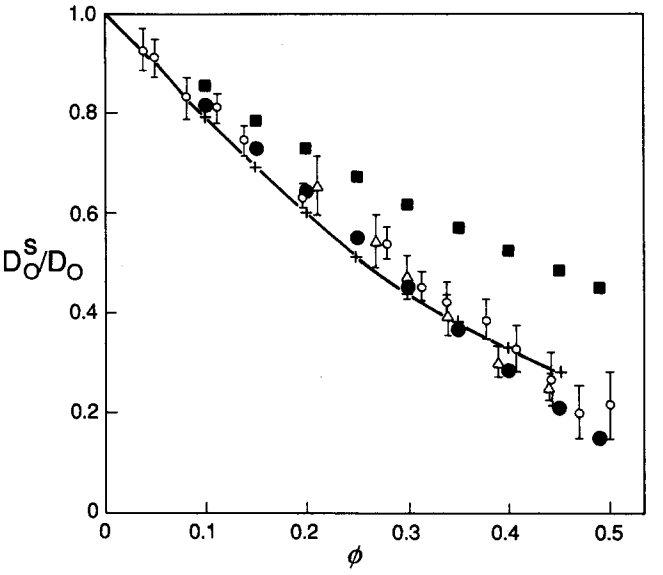

FIG. 4. Comparison of the short-time self-diffusion coefficients obtained by simulation (solid circles) with the experimental results of Ottewill and Williams (open circles) and Pusey and van Megen (open triangles), Refs. 21 and 20, respectively. Also included is a theoretical calculation of Beenakker and Mazur (Ref. 30). The solid squares are the simulation results without lubrication, showing the importance of the near-field interactions.

sion coefficient of an isolated sphere, $D_0 = kT/(6\pi\eta a)$.

In Fig. 3 we show our self-diffusion data for values of N equal to 14, 27, 32, 49, and 64. Here, a trend is clearly discernible, and assuming an $N^{-1/3}$ dependence the data have been extrapolated to $N \to \infty$ to give the solid symbols. The extrapolated results are compared in Fig. 4 with both experiment[20,21] and an alternative theory proposed by Beenakker and Mazur.[30] The agreement with theory and experiment over the entire range of volume fractions is clearly excellent. We recall here that the hard-sphere microstructure *is* the proper microstructure for the short-time self-diffusion measurements, and thus this provides a valid comparison of our Stokesian dynamics method with experiment. The effects of neglecting the near-field, lubrication interactions [i.e., leaving out $\mathscr{R}_{\text{lub}}$ in Eq. (4)] in the extrapolated values of the short-time self-diffusion coefficient are also shown in Fig. 4. In contrast to the sedimentation velocity, lubrication is clearly important in self-diffusion, as the particle of interest must push against its tightly packed neighbors in order to move. The good agreement with experiment also shows that our method of including the near-field interactions is quantitatively capturing the proper physics.

As a final point, we note that our self-diffusion coefficients extrapolated for $N \to \infty$ at low ϕ agree with Batchelor's prediction, Eq. (18), for the $O(\phi)$ coefficient. Specifically, at $\phi = 0.001$, we find a value of $D_0^s = 0.998$, while at $\phi = 0.1$, we have $D_0^s = 0.814$. These are to be compared with (18); the good agreement seems to confirm Batchelor's prediction.

Because of the pronounced effects of periodicity, which scale as $N^{-1/3}$ in this case, some readers may wonder if it is possible to use the minimum image convention without Ewald sums as a better model of a disordered system. While attractive, this approach has one serious difficulty: mobility matrices constructed with periodic boundary conditions without Ewald sums lose positive definiteness at volume fractions as low as 0.05. Nonpositive definite matrices lead to completely aphysical behavior, such as negative diffusion coefficients! Only by properly accounting for the long-range hydrodynamic interactions is the correct physics obtained.

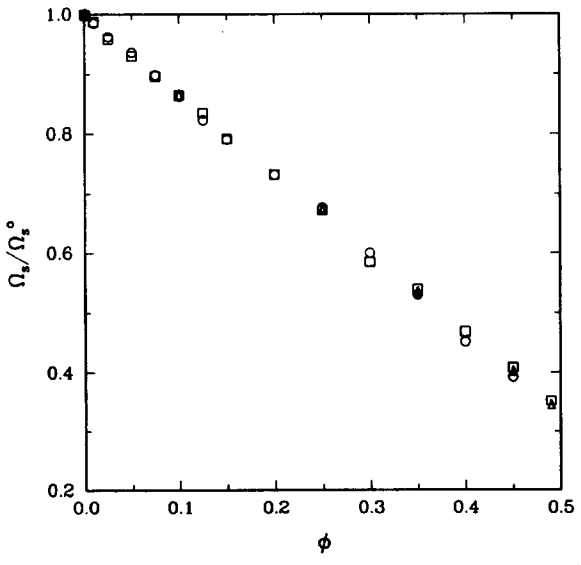

FIG. 5. The rotational velocity, normalized by its infinite dilution value, Ω_s^0, as a function of volume fraction ϕ and number of particles in the unit cell: 14 (○), 27 (□), and 64 (△). The rotational velocity is the rotational analog of the sedimentation velocity. In contrast to the sedimentation velocity, however, the finite-size effects are weak, and not detectable here [cf. Eq. (19)].

C. Rotational velocity and rotational self-diffusion coefficient

The coefficient relating the average rotational velocity to the torque, Ω_s, and the rotational self-diffusion coefficient, D_r^s, are obtained through Eqs. (7)–(9), and represent the rotational counterpart of the sedimentation velocity and translational self-diffusion coefficient discussed above. There are at present no experimental results for these quantities, and the theoretical predictions are limited to periodic systems,[12] although any of the theoretical approaches used for the translational properties could be trivially extended to the rotational case. We note here that the rotational diffusion coefficients have been measured for nonspherical particles in a variety of contexts,[31] and could be obtained for spherical particles if the particles themselves, although spherical, had an anisotropic light scattering ability. How this is to be brought about by synthesis of the particle is not readily apparent. The rotational velocities may be directly relevant to ferrofluids,[32] where small magnetic colloidal particles are caused to rotate by an applied magnetic field. (The inverse problem of the average torque produced by an average rotational velocity, which is discussed in the second paper dealing with transport properties of porous media, produces what is known as the spin viscosity and is relevant to the antisymmetric stresses generated in ferrofluids[9,12,32])

As in the translational problems, the periodic boundary

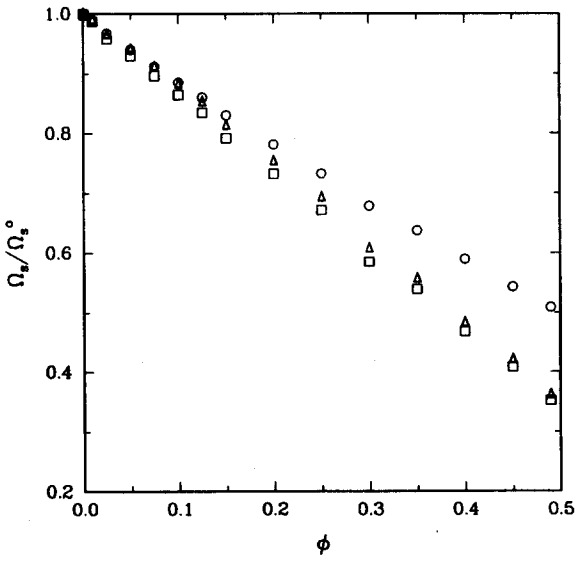

FIG. 6. Comparison of the effects of various levels of hydrodynamic interaction on the calculation of the rotational velocity. The open squares are the full F–T–S method with lubrication for 27 spheres. The open triangles are the F–T method (i.e., no stresslets, but including lubrication), and show the stresslets to have no effect on the rotational velocity. The open circles are the F–T–S method (or the F–T method) without lubrication and are given by Eq. (19): $\Omega_s/\Omega_s^0 = 1 - \phi$. Note that, in contrast to the sedimentation velocity, lubrication does play a role here as there is relative motion between particle surfaces.

conditions and Ewald sums imply that one rotating sphere in a rotational velocity calculation must necessarily be replicated by other rotating spheres arranged in an infinite SC lattice. In Fig. 5 our results for rotational velocities calculated with N equal to 14, 27, and 64 spheres are shown. The fact that the three sets of results are essentially identical indicates that periodicity is not an important factor in this calculation. To explain this observation, we follow the approach used to assess the periodicity effects in the sedimentation velocity, and look for a low volume fraction solution for Ω_s. The solution provided by Zuzovsky *et al.*[12] for an SC lattice of rotating spheres is *independent* of structure for very dilute systems:

$$\Omega_s = 1 - \phi. \tag{19}$$

The fact that Eq. (19) is valid for both periodic and disordered systems suggests that the effect of a rotating sphere's periodic self-reflections, all of which are at least one periodic box length away from the central sphere, is no different than if they were located at random positions. Clearly this argument is supported by the data shown in Fig. 5. The finite-size effects should thus scale at most as N^{-1}, and may, in fact, not be present. Normally, when the same dependence to leading order in ϕ is found for random and periodic suspensions, the periodically replicated disordered systems give the proper result independent of N, i.e., there are no finite-size effects. However, it is known from the work of Durlofsky and Brady[33] that the resistance matrix formed from the mobility invert has $O(N^{-1})$ errors owing to the effects of the periodic boundary conditions on the satisfaction of overall mass and/or momentum balances. Thus these $O(N^{-1})$ errors may also be present in the rotational mobility problems, and we give the conservative estimate that the finite-size effects scale as N^{-1}. We have not extrapolated the data in Fig. 5 with this scaling as the resulting values would lie within the error bars for the $N = 64$ results.

In Fig. 6, rotational velocities calculated using the F–T method and using the F–T–S method without including lubrication are shown. As one would expect, the stresslets, which result from a symmetric distribution of force density about the particle surfaces, have only a slight effect on the rotational velocities. Note also that the results with no lubrication fall precisely along the line given by Eq. (19), showing that the far-field interaction terms alone give rise to the dilute limit result. One can also see from Fig. 6 that, in contrast to the sedimentation velocity, lubrication does play an important role in the rotational velocity calculations. This is due to the fact that, in this case, there is relative motion between particle surfaces, and thus as spheres approach one another lubrication has a considerable effect.

In Fig. 7 and 8 we present the results for D_r^s, the short-time rotational self-diffusion coefficient normalized by the rotational diffusion coefficient for an isolated sphere, $D_r^0 = kT/(8\pi\eta a^3)$. Again, Fig. 7 shows that periodicity effects are negligible for this calculation. To explain why this is the case, we can do an analysis similar to that just discussed. From Eq. (19) we know that the rotating sphere's reflections hinder its motion by ϕ/N, while we assume that the effect of the neutrally buoyant spheres can be accounted for by an effective viscosity that grows like $\frac{5}{2}(1 - 1/N)\phi$ (Einstein's low ϕ viscosity result). Thus our criterion for neglecting periodicity effects is

$$(\phi/N)/\tfrac{5}{2}\phi(1 - 1/N) \approx 0.4/N \ll 1, \tag{20}$$

an inequality that is satisfied in all of our simulations. Again, the finite-size effects scale as N^{-1}.

Unlike the rotational velocity calculations, however, from Fig. 8 one can see that the stresslets are important here. The reason for this should be clear: in a suspension of spheres that have no applied forces or torques, the only far-field quantities left to interact with a single rotating sphere are the stresslets, in the absence of which it can only interact with its

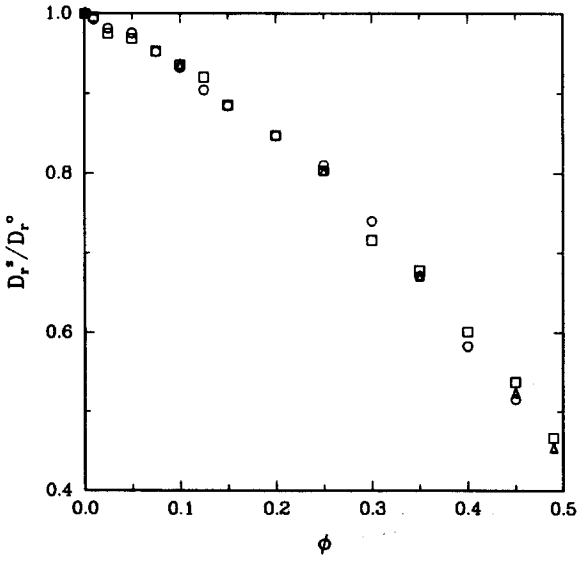

FIG. 7. The short-time rotational diffusion coefficient normalized by the rotational diffusion coefficient of an isolated sphere, $D_r^0 = kT(8\pi\eta/a^3)$, is plotted versus ϕ for three different numbers of particles in the unit cell: 14 (○), 27 (□), and 64 (△). As in the rotational velocity case, the finite-size effects are weak and are almost imperceptible in the figure.

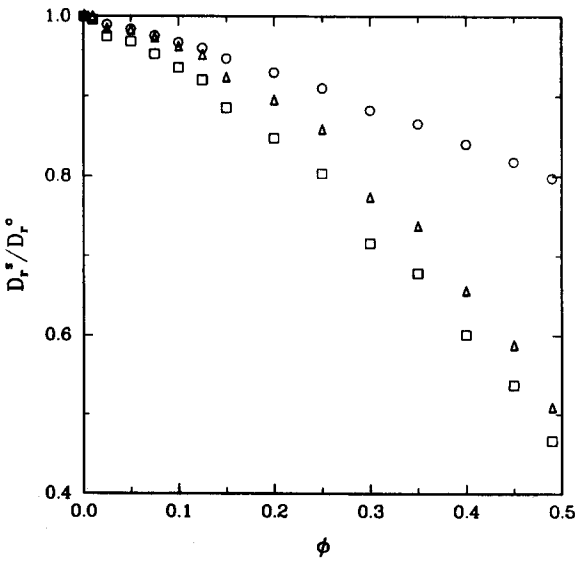

FIG. 8. Comparison of various levels of hydrodynamic approximation on the rotational diffusion coefficient. The open squares are the full F–T–S method results for 27 spheres, the open triangles are the F–T method results (no induced stresslets), and the open circles are the F–T–S method results without lubrication.

own periodic images. Indeed, although these data were left out for simplicity, if the F–T results that do not include lubrication effects were plotted, they would be identically reproduced by $(1-\phi/N)$, which is just the result given by (19) for an SC lattice of spheres in an otherwise pure fluid. This behavior underscores the importance of stresslets in determining the average properties of suspensions.

D. Effective viscosity

The effective viscosity of a suspension of force- and torque-free particles is determined by the suspension average stresslet of Eq. (10). For a random dispersion at low volume fraction we have

$$\eta_r = 1 + \tfrac{5}{2}\phi + 5.07\phi^2, \tag{21}$$

where the $\frac{5}{2}\phi$ is from Einstein's result, and the $O(\phi^2)$ coefficient is from Batchelor and Green.[6,2] Since the $O(\phi)$ coefficient is independent of structure, just as was the case for the rotational velocity [cf. Eq. (19)], the finite-size effects are at most $O(N^{-1})$. The same scaling in the two cases is to be expected since both the torque and stresslet are first moments of the force distribution on the surface of a particle.

This scaling (or its weak dependence on N) is borne out in Fig. 9 where the relative viscosity determined by the F–T–S method is plotted versus ϕ for N equal to 14, 27, and 64. Also shown in the figure are the low ϕ asymptotic result and two correlations given by Krieger.[34] The upper curve of Krieger corresponds to the limit of low (steady) shear rate (low Peclet number), while the lower curve corresponds to the limit of high shear rate (high Peclet number). One should view these curves as simply giving an idea of where the experimental data lie in relation to our simulation results.

In general, agreement between experiment, our simulation results, and the low ϕ asymptotic result is quite good up to $\phi = 0.15$, which may be taken as a confirmation of the calculation of Batchelor and Green. At higher ϕ, both simulation and experiment lie significantly above the low ϕ asymptote and increase rapidly with increasing ϕ.

Although our simulation results compare favorably with Krieger's high Peclet number asymptote, caution must be exercised in making a direct comparison between theory and experiment in this case. At low shear rates, Brownian motion has a strong randomizing effect, and our microstructure (equilibrium hard sphere) is close to that of the slightly deformed low Peclet number limit suspension, corresponding to the upper curve of Krieger. Hence one may think that our results should be compared with these data. However, there is an additional direct Brownian contribution to the bulk stress that can only be obtained by calculation of the deformed microstructure. Recent simulations[14] indicate that this contribution is about equal in magnitude to the purely hydrodynamic part calculated here. Thus our simulation results should fall well below the upper curve of Krieger. This Brownian contribution decreases with increasing shear rate (shear thinning), explaining the lowering of the curve for high shear rates. At high shear rates, however, the suspension microstructure is far from being a hard-sphere distribution. Considerations of clustering observed under these conditions[7,17] indicate that the viscosity corresponding to the equilibrium, hard-sphere distribution is lower than that corresponding to the actual microstructure that develops at high shear rates. Hence the reasonable agreement in magnitude and general trends suggests that our Stokesian dynamics method is capturing the proper physics.

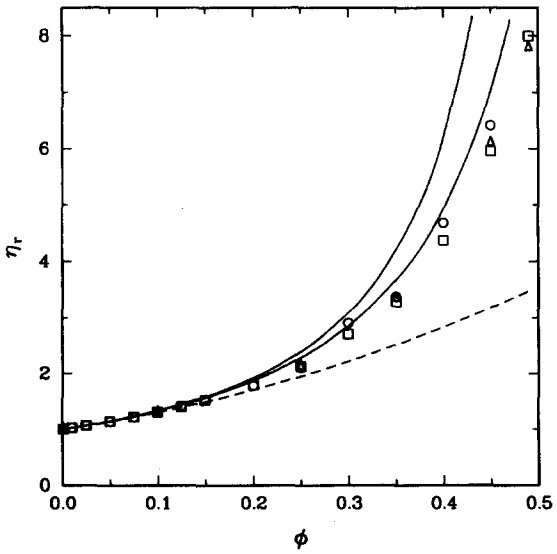

FIG. 9. The relative viscosity, η_r, defined as the suspension viscosity determined from Eqs. (10)–(13) nondimensionalized by the fluid viscosity, is plotted as a function of the volume fraction (ϕ) for several cases. The open symbols are the Stokesian dynamics results for 14 (○), 27 (□), and 64 (△) spheres, showing the insensitivity of the results to system size. The dashed curve is the low ϕ theoretical result of Batchelor and Green (Ref. 6), and the solid curves are correlations of experimental data from Krieger (Ref. 34). The upper, solid curve corresponds to the low Peclet number limit, while the lower curve corresponds to the high Peclet number limit of the steady shear viscosity.

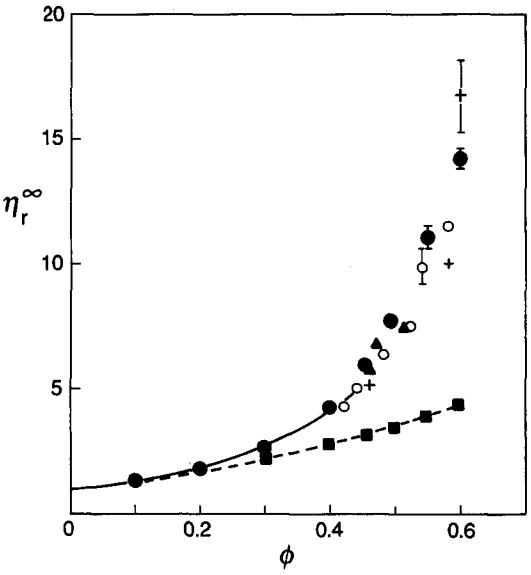

FIG. 10. Comparison of the simulation viscosities (for 27 and 32 particles, solid circles) with the experimentally measured high-frequency dynamic viscosities (η_r^∞) reported by van der Werff *et al.* (Ref. 22); the experiments were for monodisperse hard spheres of radii 28 nm (+), 46 nm (○), and 76 nm (▲), respectively. The solid line is a theoretical prediction by Beenakker (Ref. 36). The dashed line is the low ϕ asymptotic prediction of Batchelor and Green (Ref. 6), which agrees remarkably well with the simulation method without lubrication (solid squares) over the entire range of ϕ.

There is an experimental situation which does correspond to the viscosity calculated in our simulations. In high-frequency, low amplitude shearing of Brownian suspensions, the microstructure is only slightly deformed from the hard-sphere structure used here, and the direct Brownian contribution is out of phase with the applied oscillating shear field, resulting in a shear modulus of elasticity.[35] Thus in the limit of small (i.e., linear) deformation, the dynamic viscosity corresponds to our Monte Carlo, hard-sphere viscosities. In Fig. 10, we show a comparison of our results with the high-frequency experiments of van der Werff *et al.*[22] The agreement is quite satisfactory considering the sensitivity of the results to slight changes in ϕ. This should serve to confirm the quantitative accuracy of the Stokesian dynamics method. Because van der Werff *et al.* provide experimental data for systems with $\phi > 0.49$, we have included in Fig. 10 simulation results for $\phi = 0.55$ and $\phi = 0.60$. The error bars on these points are given by the standard error, i.e., the standard deviation of our set of 50 results (five values from each of the ten samples used) divided by the square root of 50. The relatively large standard deviations associated with these points can be attributed to the presence of clusters of particles which vary in size from one sample to another, and hence cause large fluctuations in η_r. A macroscopic system at these high values of ϕ would undoubtedly have clusters in some regions and freely mobile particles in others, a situation that is difficult to model with the number of particles considered here. More accurate results could be obtained by performing simulations with enough particles to model the complete structure. At present, however, computer time limitations would make such an endeavor unfeasible. Finally, we note in passing that the experimental results of van der Werff *et al.* show the proper hydrodynamic scaling with particle size and shear rate for all volume fractions up to ϕ in excess of 0.7 even for particles as small as 28 nm, indicating that the continuum mechanical description for smooth, hard spheres applies down to remarkably small particle surface–surface separations.

The effects of neglecting lubrication on our simulation calculations and the theoretical results of Beenakker[36] are also shown in Fig. 10. Remarkably, the low ϕ result (21) agrees with our far-field result all the way up to $\phi = 0.60$. All the deviation from (21) and the rapid rise with increasing ϕ is accounted for by the pairwise additive, near-field lubrication interactions. Beenakker has developed the most rigorous theory available for the viscosity of a suspension with the hard-sphere microstructure (high-frequency viscosity), and his results agree well both with ours and with the experimental results up to a volume fraction of $\phi \simeq 0.4$. At higher volume fractions, both experimental results and our simulation results continue to rise rapidly as the lubrication singularities gain importance. Beenakker's theory, while quite accurate, evidently does not incorporate enough of the near-field structure and interactions to obtain a high viscosity.

The form of the viscosity, both experimentally and in our simulations, suggests a singular behavior at a critical volume fraction in excess of $\phi = 0.6$. This has been noted, and theoretical descriptions of this behavior have been attempted by many authors. Unfortunately, we must leave this question unanswered at the present time and hope we will be able to address it in the future.

V. CONCLUSIONS

The primary purpose of this paper was to present our Stokesian dynamics results on the hydrodynamic transport properties of hard-sphere dispersions. The hard-sphere distribution represents a convenient reference microstructure, and one should view these results almost as "experimental" data. We hope they can play a role in developing theories and understanding of suspension properties much the same way conventional molecular dynamics has aided the development of liquid state theory. Indeed, one may use these results to start a "perturbation theory" of suspensions similar to liquid state perturbation theory. This approach has actually been started at the low Peclet number limit,[35] and we have recently used simulations to help test these perturbation theories.[37]

The comparisons we have made with experiment have been as complete as possible. We have seen that our sedimentation velocities do not agree particularly well with experiment, owing to the severe effects of periodicity at low volume fractions and the need for higher-order many-body multipole moments at higher volume fractions (cf. Fig. 1). These problems could be eliminated at increased computational cost, but hardly seem worth the effort. An understanding of the behavior is the important aspect and, in conjunction with our other work on sedimentation,[9,29] we feel that this understanding has been obtained.

Our comparisons with the effective viscosity and self-diffusion coefficient have been much more favorable. The effective viscosity results lie near, but below, the experimental data corresponding to steady shear as expected and as explained in Sec. III (cf. Fig. 9); experimentally measured high-frequency dynamic viscosities are, however in very good agreement with our simulation results (cf. Fig. 10). Our self-diffusion coefficients are also in excellent agreement with experiment (cf. Fig. 4). We recall here that for the latter two cases the hard-sphere distribution is the correct microstructure, and thus they provide a rigorous test of our hydrodynamics. Comparison with the rotational properties (velocity and self-diffusion) must await experimental measurement.

We have not made an exhaustive comparison with all the available theories, as this was not our purpose. Such a study is best done in the course of a review paper. We have compared our results with the dilute solution theories of Batchelor and have generally found excellent agreement, the notable exception being the low ϕ, limiting behavior of the sedimentation velocity. The only other theories which we have used for purposes of comparison are those of Beenakker. His theories for the self-diffusion coefficient and dynamic viscosity are the most complete and rigorous available and are in excellent agreement with our simulations up to volume fractions of about 0.4. At higher ϕ, evidently more interactions need to be included in Beenakker's analyses. Nevertheless, his theories represent a remarkable accomplishment.

As a by-product of our study, we have determined the scaling with number of particles for the finite-size effects resulting from the use of periodic boundary conditions. These effects are most severe for the sedimentation velocity and self-diffusion coefficient, where the scaling is an extremely slow $N^{-1/3}$. This behavior makes it somewhat difficult, although not impossible, to extract the $N \to \infty$ limiting results. On the other hand, for the rotational properties and the effective viscosity, the finite-size effects scale at most as N^{-1} (see also Durlofsky and Brady[33]). It is thus only the translational properties of free suspensions that are adversely affected by the periodicity. There are, of course, other constraining effects of the periodicity, such as fitting all important microstructure length scales within the periodic box, that are not related to the long-range nature of the hydrodynamic interactions discussed here.

We have limited the majority of our study to volume fractions below 0.49, because above this value the hard-sphere suspension undergoes a fluid–solid phase transition. It is of interest, particularly for the shear viscosity, to continue to higher volume fractions into a disordered, glassy state. This we shall do in a future communication.

We hope we have provided a set of results for the hydrodynamic transport properties of the hard-sphere microstructure that will be of use in testing both theory and experiment on dense suspension behavior. We also hope that our comparisons of various levels of hydrodynamic approximation have given some new insights into suspension mechanics and may help to stimulate new developments in the future.

ACKNOWLEDGMENTS

We wish to thank our colleague L. Durlofsky for helpful discussions on the Stokesian dynamics method and on the role of induced stresslets in suspension mechanics.

This research was supported in part by National Science Foundation Grants No. CBT-8696067 and No. INT-8413695. Computer time was provided by the von Neuman Supercomputer Center. RJP would also like to acknowledge the support of a NSF fellowship.

[1] D. J. Jeffrey and Y. Onishi, J. Fluid Mech. **139**, 261 (1984).
[2] S. Kim and R. T. Mifflin, Phys. Fluids **28**, 2033 (1985); B. J. Yoon and S. Kim, J. Fluid Mech. **185**, 437 (1987).
[3] G. K. Batchelor, J. Fluid Mech. **52**, 245 (1972).
[4] G. K. Batchelor, J. Fluid Mech. **74**, 1 (1976).
[5] A. B. Glendinning and W. B. Russel, J. Colloid Interface Sci. **89**, 124 (1982).
[6] G. K. Batchelor and J. T. Green, J. Fluid Mech. **56**, 401 (1972).
[7] J. F. Brady and G. Bossis, J. Fluid Mech. **155**, 105 (1985).
[8] L. Durlofsky, J. F. Brady, and G. Bossis, J. Fluid Mech. **180**, 21 (1987).
[9] J. F. Brady, R. J. Phillips, J. C. Lester, and G. Bossis, J. Fluid Mech. **195**, 257 (1988).
[10] A. Zick and G. M. Homsy, J. Fluid Mech. **115**, 13 (1982).
[11] K. C. Nunan and J. B. Keller, J. Fluid Mech. **142**, 269 (1984).
[12] M. Zuzovsky, P. M. Adler, and H. Brenner, Phys. Fluids **26**, 1714 (1983).
[13] J. F. Brady and G. Bossis, Annu. Rev. Fluid Mech. **20**, 111 (1988).
[14] G. Bossis and J. F. Brady, submitted to J. Chem. Phys.
[15] L. Durlofsky and J. F. Brady, to appear in J. Fluid Mech.
[16] G. Bossis and J. F. Brady, J. Chem. Phys. **80**, 5141 (1984).
[17] G. Bossis and J. F. Brady, J. Chem. Phys. **87**, 5437 (1987).
[18] R. J. Phillips, J. F. Brady, and G. Bossis, Phys. Fluids **31**, 3473 (1988).
[19] W. G. Hoover and F. H. Ree, J. Chem. Phys. **49**, 3609 (1968).
[20] P. N. Pusey and W. van Megen, J. Phys. (Paris) **44**, 285 (1983).
[21] R. H. Ottewill and N. St. J. Williams, Nature **325**, 232 (1987).
[22] J. C. van der Werff, C. G. de Kruif, C. Blom, and J. Mellema, in *Proceedings of the Fourth EPS Liquid State Conference*, Arcachon, France (M. Nijhoff, Amsterdam, 1989).
[23] K. Binder, *Monte Carlo Methods in Statistical Physics* (Springer, New York, 1986).
[24] J. A. Barker and D. Henderson, Mol. Phys. **21**, 187 (1971).
[25] R. W. O'Brien, J. Fluid Mech. **91**, 17 (1979).
[26] In all three methods, we have included a mean-field quadrupole contribution (see Ref. 9 for details), so that all remaining interactions are absolutely convergent.
[27] P. G. Saffman, Stud. Appl. Math. **52**, 115 (1973); H. Hasimoto, J. Fluid Mech. **5**, 317 (1959).
[28] R. Buscall, J. W. Goodwin, R. H. Ottewill, and F. Tadros, J. Colloid Interface Sci. **85**, 78 (1982).
[29] J. F. Brady and J. Durlofsky, Phys. Fluids **31**, 717 (1988).
[30] C. W. J. Beenakker and P. Mazur, Physica A **126**, 349 (1984).
[31] B. J. Berne and R. Pecora, *Dynamic Light Scattering* (Wiley, New York, 1976).
[32] R. E. Rosensweig, *Ferrohydrodynamics* (Cambridge, New York, 1987).
[33] L. Durlofsky and J. F. Brady, Phys. Fluids **30**, 3329 (1987).
[34] I. M. Krieger, Adv. Colloid Interface Sci. **3**, 111 (1972).
[35] W. B. Russel and A. Gast, J. Chem. Phys. **84**, 1815 (1986); see also the corrections to this theory in M. W. F. van Iersel, M. S. thesis, Princeton University, 1987.
[36] C. W. J. Beenakker, Physica A **128**, 48 (1984).
[37] G. Bossis, J. F. Brady, and C. Mathis, J. Colloid Interface Sci. (in press).